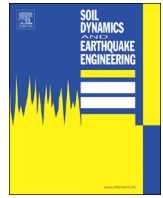




ELSEVIER

Contents lists available at ScienceDirect

## Soil Dynamics and Earthquake Engineering

journal homepage: [www.elsevier.com/locate/soildyn](http://www.elsevier.com/locate/soildyn)

## Field testing and analysis of high speed rail vibrations

D.P. Connolly<sup>a,\*</sup>, G. Kouroussis<sup>b</sup>, P.K. Woodward<sup>a</sup>, P. Alves Costa<sup>c</sup>, O. Verlinden<sup>b</sup>, M.C. Forde<sup>d</sup><sup>a</sup> Heriot-Watt University, Institute for Infrastructure & Environment, Edinburgh, UK<sup>b</sup> Department of Theoretical Mechanics, Dynamics and Vibrations, University of Mons, 31 Boulevard Dolez, B-7000 Mons, Belgium<sup>c</sup> University of Porto, Faculty of Engineering, Porto, Portugal.<sup>d</sup> University of Edinburgh, Institute for Infrastructure and Environment, School of Engineering, AGB Building, The Kings Buildings, Edinburgh, UK

## ARTICLE INFO

## Article history:

Received 20 May 2014

Received in revised form

29 August 2014

Accepted 31 August 2014

Available online 26 September 2014

## Keywords:

High speed rail

Railway

Vibration prediction

Ground borne vibration

Download data

Embankment

Cutting

Environmental impact assessment

EIA

Ground-borne noise

Experimental testing

MASW

In-situ testing

## ABSTRACT

This paper outlines an experimental analysis of ground-borne vibration levels generated by high speed rail lines on various earthwork profiles (at-grade, embankment, cutting and overpass). It also serves to provide access to a dataset of experimental measurements, freely available for download by other researchers working in the area of railway vibration (e.g. for further investigation and/or the validation of vibration prediction models).

First, the work outlines experimental investigations undertaken on the Belgian high speed rail network to investigate the vibration propagation characteristics of three different embankment conditions. The sites consist of a 5.5 m high embankment, an at-grade section and a 7.2 m deep cutting. The soil material properties of each site are determined using a 'Multichannel Analysis of Surface Waves' technique and verified using refraction analysis. It is shown that all sites have relatively similar material properties thus enabling a generalised comparison.

Vibration levels are measured in three directions, up to 100 m from the track due to three different train types (Eurostar, TGV and Thalys) and then analysed statistically. It is found that contrary to commonly accepted theory, vertical vibrations are not always the most dominant, and that horizontal vibrations should also be considered, particularly at larger offsets. It is also found that the embankment earthworks profile produced the lowest vibration levels and the cutting produced the highest. Furthermore, a low (positive) correlation between train speed and vibration levels was found. A selection of the results can be downloaded from [www.davidpconnolly.com](http://www.davidpconnolly.com).

© 2014 Elsevier Ltd. All rights reserved.

## 1. Introduction

The rapid uptake of high speed rail has been in-part due to its superior economic, social and environmental benefits [6] in comparison to other modes of transport. On-going research into aerodynamics, construction materials and motor technology has allowed for the development of lightweight trains capable of reaching increasingly higher speeds. Japan holds the world record for the fastest high speed rail velocity of 581 km/h which is close to the speed experienced by a typical commercial jet.

One negative environmental side effect of high speed rail is the elevated levels of ground-borne vibration generated [7]. These vibrations are generated at the wheel/rail interface and arise from

the train weight (quasi-static excitation), from changes in support stiffness (e.g. regularly spaced sleepers) and irregularities in the wheel/rail geometry (dynamic excitation) [50,12]. Additionally, vibration amplitude levels may be elevated if the train speed becomes comparable with the natural Rayleigh wave speed in the supporting soil [17,21,24,37,43], or if the excitation frequency is close to a track natural frequency [23].

These vibrations can cause significant negative effects such as personal distress in communities residing close to the lines. Therefore it is important to predict vibration levels before the line is constructed [11,13]. A vast body of prediction models has been proposed for investigating vibration levels on at-grade track sections [3,15,26,36,37,40,47,51] and underground lines [1,27,29,30,42,45,52]. Despite this, research related to railway vibrations under different earthwork profile conditions is scarce.

An advantage of an experimental study over a numerical one is that a reduced number of modelling assumptions are required. For example, [20] presented an analytical model for the investigation of vibrations due to an embankment and it was shown that the

\* Corresponding author.

E-mail addresses: [d.connolly@hw.ac.uk](mailto:d.connolly@hw.ac.uk) (D.P. Connolly), [georges.kouroussis@umons.ac.be](mailto:georges.kouroussis@umons.ac.be) (G. Kouroussis), [p.k.woodward@hw.ac.uk](mailto:p.k.woodward@hw.ac.uk) (P.K. Woodward), [pacosta@fe.up.pt](mailto:pacosta@fe.up.pt) (P. Alves Costa), [olivier.verlinden@umons.ac.be](mailto:olivier.verlinden@umons.ac.be) (O. Verlinden), [m.forde@ed.ac.uk](mailto:m.forde@ed.ac.uk) (M.C. Forde).

embankment was a source of high frequency vibration. Despite this, the embankment was assumed to have vertical sides and the train excitation was uncoupled from a simplified track model. Another approach was presented by [8] who used a 3D finite element (FE) modelling approach to analyse vibrations within embankments with varying stiffness. It was shown that stiff embankments provided superior vibration performance in comparison to soft ones. A drawback of the FE approach is that assumptions must be made concerning the distribution of soil properties, and high frequency content can be difficult to simulate.

To overcome some of the limitations associated with numerical analysis [18,25,31,32], performed experimental analysis on at-grade railway tracks to analyse the characteristics of railway vibration. Despite this, few investigations have been undertaken into embankment vibration. One of the few studies used accelerometers to record ground movement on the rail, sleeper and an embankment made from compacted gravel [39]. It was found that the dominant frequencies within the embankment were between 40 and 70 Hz, with the spectrum reducing in frequency with distance from the embankment shoulder. Unfortunately the results were not compared to non-embankment data.

To the authors' knowledge, there is no published literature related to the experimental analysis of vibration from railway cuttings. Therefore this paper attempts to compare the vibration levels generated by cuttings, embankments and at-grade track sections, via field experiments [10,33]. First, experimental investigations are performed at three Belgian test sites. Vibration levels are recorded in all three component directions and vertical vibrations are recorded up to a distance of 100 m from the track. All sites are found to consist of similar soil characteristics as determined through Multichannel Analysis of Surface Waves (MASW) testing, thus allowing for a general comparison between vibration characteristics. In addition to earthwork profile conditions, the effect of train type, horizontal vibration and abutment presence are investigated. A key aim of this paper is to provide a series of vibration records that researchers can use for further

investigation and for the validation of numerical prediction models.

## 2. Test site details

### 2.1. General

#### 2.1.1. Site 1—At-grade

Site 1 consisted of an at-grade railway section (Figs. 1 and 2) 4 km south of the town of Leuze-en-Hainaut. The track was a classically ballast track composed of ballast, subballast and sub-grade layers, with thicknesses 0.3, 0.2 and 0.5 m, respectively. The rails were continuously welded UIC 60 rails with a mass of 60 kg/m<sup>3</sup> and fixed to the prestressed concrete sleepers (300 kg monoblock) via Pandrol clips (Fig. 3). The rails were also supported by railpads with thickness 0.01 m. The irregularity of the rails (for all test sites) was assumed to be very low because grinding had been performed eight days before testing. It was also assumed that the standard of track geometry was high and identical across all test sites.

Two distinct test setups were deployed, the first to record three component vibration levels at distances of 9–35 m from the closest track (Table 1), and the second to record vertical vibration between 9 and 100 m from the track (Table 2). The first setup was composed of 8 low frequency, 3 component, SM-6 geophones, with sensitivity 28.8 V/m/s (Fig. 4). For the second setup, 24 low frequency, 1 component (vertical), SM-6 geophones, also with sensitivity 28.8 V/m/s were used.

During post-processing, for each velocity time history recorded, the low frequency content was amplified by multiplying it by the inverse of the geophone response curve. This 'corrected' the geophone response which otherwise would have inaccurately recorded frequency content below 4.5 Hz.



Fig. 1. At-grade track section.

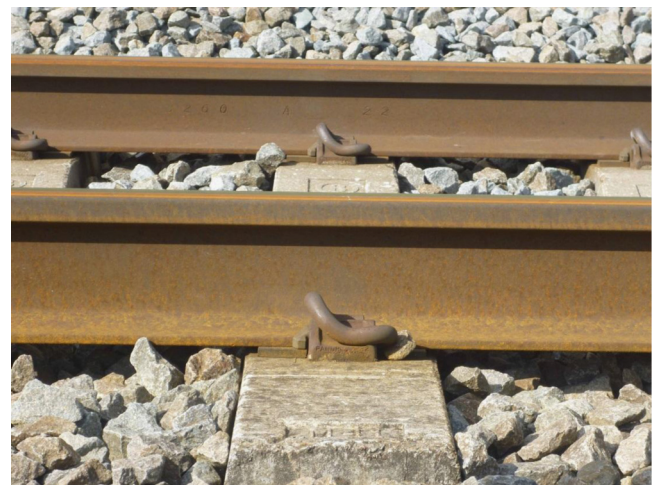


Fig. 3. Ballasted track configuration (all sites).

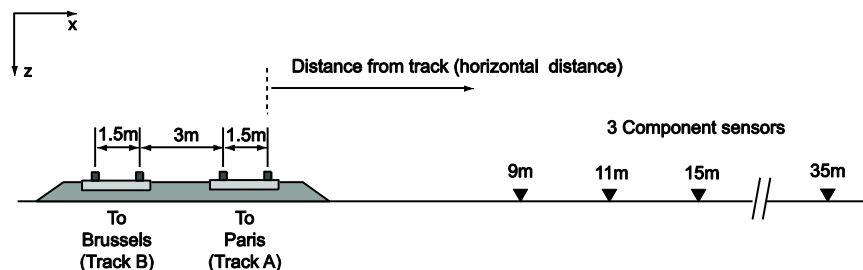


Fig. 2. At-grade track section geophone configuration.

**Table 1**  
Three component geophone distances.

Distance from rail (m)	3 Component measurements								
	9	11	15	19	23	27	31	35	
Component(s) measured <sup>a</sup>	H1, H2, V1	H1, H2, V1	H1, H2, V1	H1, H2, V1	H1, H2, V1	H1, H2, V1	H1, H2, V1	H1, H2, V1	H1, H2, V1

<sup>a</sup> H1=Horizontal component, H2=horizontal component, V1=vertical component.

**Table 2**  
One component geophone distances.

Distance from rail (m)	1 Component measurements											
	9	11	13	15	21	25	29	33	37	41	45	49
Component(s) measured <sup>a</sup>	V1	V1	V1	V1	V1	V1	V1	V1	V1	V1	V1	V1
Distance from rail (m)	53	57	61	69	73	77	81	85	89	93	97	100
Component(s) measured <sup>a</sup>	V1	V1	V1	V1	V1	V1	V1	V1	V1	V1	V1	V1

<sup>a</sup> V1=vertical component.



**Fig. 4.** In-field deployment of a three component geophone.



**Fig. 5.** Embankment track configuration.

#### 2.1.2. Site 2—Embankment

Site 2 was also located on the Paris–Brussels line, North-East of the town of Braffe. The track configuration consisted of an embankment 5.5 m high with a slope of 30 degrees (Figs. 5 and 6). The experimental methodology and geophone arrangement was consistent with site 1.

#### 2.1.3. Site 3—Cutting

Site 3 was also located on the Paris–Brussels line, North-West of the town of Braffe (Figs. 7 and 8). The track configuration consisted of a cutting (excavated embankment), 7.2 m high at a gradient of 25 degrees. The track components were identical that of test site 1.

#### 2.1.4. Site 4—Abutment

Site 4 was located approximately 100 m East of site 2 and thus the track components were identical that of test site 2. The embankment was also identical to site 2 except that there was a concrete under-pass passing through the embankment and beneath the track.

This under-pass served as a minor road for car passage and is shown in Fig. 9. At this site a hybrid geophone setup was deployed, combining aspects of both of the previously described setups.

#### 2.2. Train characteristics

Four train set configurations were recorded across all sites during the measurement campaign: TGV, Eurostar, Thalys and double-Thalys. A brief description of each train follows, with the majority of train properties obtained from Ref. [35]. Sample time histories from the passage of a Thalys train are shown in Fig. 14.

##### 2.2.1. TGV Réseau (TGV)

TGV train-sets are manufactured by Alstom and commenced commercial operation in 1993. The TGV-R is the successor to the TGV Atlantique. During testing, each train-set consisted of two power cars at each end (Y230A), six passenger cars in the centre (Y237A) and two lateral cars (Y237B) connecting the power and passenger cars. Bogies were shared between passenger cars and the power cars had two separate bogies each (Fig. 10). Table 3 shows the specification of the TGV train-set.

##### 2.2.2. Thalys and Thalys double (Thalys)

Thalys high speed train sets commenced operation on European high speed lines in 1998 and have a maximum commercial speed of 300 km/h. They are derived from the TGV and manufactured by Alstom. The total train length spans 200 m. Double Thalys train sets use identical cars as the single Thalys, however there is twice the number of passenger cars. The layout and configuration of the Thalys locomotives is shown in Figs. 11 and 12 and Table 4.

##### 2.2.3. Eurostar TransManche (Eurostar)

The Eurostar was manufactured by Alstom and has been operational since 1993. Its length of 394 m makes it longer than both the Thalys and TGV and it is capable of holding 750 passengers. In common with the Thalys and TGV train-sets, wheel spacing is identical and it consists of three car types: driving cars at the ends, lateral cars next to the driving cars and passenger cars in the middle. The entire train-set consists of 20 carriages. Wheel

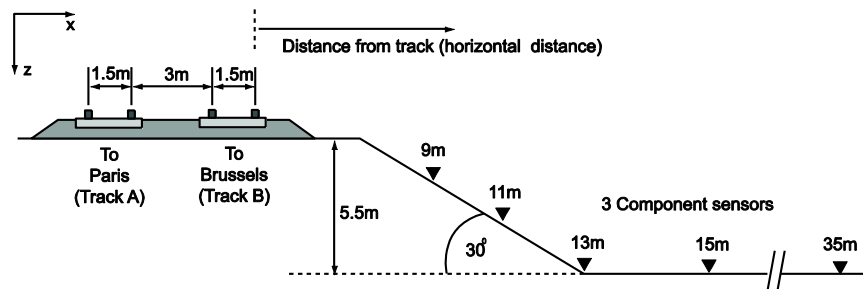


Fig. 6. Embankment track section geophone configuration.



Fig. 7. Cutting track section.

layout is shown in Fig. 13 and the train-set specifications are shown in Table 5.

#### 2.2.4. Train speed calculation

Approximate train speeds were obtained using information provided by the train operator, Infrabel. In an attempt to maximise accuracy, train speeds were also determined independently using a newly developed calculation procedure [34]. This procedure used a combination of cepstral analysis, dominant frequency analysis and a regression analysis (based upon minimising the error between experimental frequencies and an analytical quasi-static excitation solution). Although all three approaches varied in nature, the underlying methodology was similar, i.e. to isolate the key vehicle frequencies (Fig. 15) and use them to calculate the train speed. For all the high speed train speeds computed in this study it was found that although all three techniques worked well, it was sufficient to focus on using cepstral analysis. If speed information was required for alternative train types (e.g. freight) then this may not have been the case. After analysis, it was found that for all 56 recorded train passages, the minimum speed was 280.1 km/h, the maximum speed was 303.6 km/h, and the average train speed was 294.7 km/h.

### 2.3. Ground dynamic characterisation

To determine the material properties of the soils at each test site, MASW was used in conjunction with a desktop survey of existing soils data.

#### 2.3.1. Experimental setup

The MASW experimental setup is shown in Fig. 16. Excitation was provided using a 12lb PCB 086D50 impact hammer with on-board accelerometer. The accelerometer was connected to a data acquisition unit using a microdot connector. This allowed for calculation of the input force exerted by each hammer blow.

Twenty four low frequency (4.5 Hz), vertical component, SM-6 geophones were placed parallel to the railway track, in the same line as the geophones used for recording train vibrations. The

array was placed far enough away from the track to ensure the results were not contaminated from potential artefacts close to the line, but close enough to ensure that the soil properties were representative of those beneath the track. No MASW measurements were undertaken during train passage.

Geophone spacing was 1 m as recommended by [44] and each sensor was coupled to the ground using 150 mm spikes [48]. Excitation was performed at 7 individual locations by striking an embedded metal impact plate. All results were amplified using a high gain setting and recorded using a Panasonic Toughbook in SEG-2 format. The gain was removed during post-processing.

#### 2.3.2. Multichannel analysis of surface waves

The MASW results were analysed using Geopsy [54] and sub-program Dinver [53]. Geopsy is a graphical user interface (GUI) capable of generating dispersion curve plots from recorded signals. From these plots, the best fit dispersion curves were chosen visually and exported for use in sub-program Dinver.

To perform the inversions using Dinver, density was held constant at 2000 kg/m<sup>3</sup>. Shear wave (S-wave) speed is highly independent of density and therefore density is typically held constant to increase the accuracy and reliability of the MASW process. Inversion was then used to calculate the layer depths and wave speeds of the underlying soil. Compressional wave (P-wave) profiles were validated using a refraction analysis, performed using the commercial seismic software package, SiesImager/2D. The sub-module PickWin was used to identify first arrivals and sub-module Plotrefa was used to calculate the P-wave velocity profile. Geopys MASW results were found to be consistent with SeisImager results.

As an additional check, a desktop study was undertaken by comparing results to existing soil information. For sites 1–4, generalised soil maps were available describing the soil layer permutations and composition of each layer. For all sites, the experimental findings were generally consistent with the existing records. Once the wave speeds had been determined with confidence, the Young's modulus was calculated using elementary material property relationships.

#### 2.3.3. Classification of soil properties

Fig. 17 describes the soil properties associated with each test site (for further details see Appendix). As test site 4 was in very close proximity (< 100 m) to test site 2 (Belgian embankment site), no MASW tests were undertaken and the soil properties were assumed to be identical to site 2.

The resulting soil properties were in good agreement with existing soil records from the area and were also similar to those presented by [36] for previous spectral analysis of surface waves (SASW) tests undertaken on nearby soils. Fig. 17 shows that the soil properties at all three sites were similar in regards to wave speed profile and layer depth/orientation. The only inconsistency was at site 3 which was underpinned by a layer of clay that was

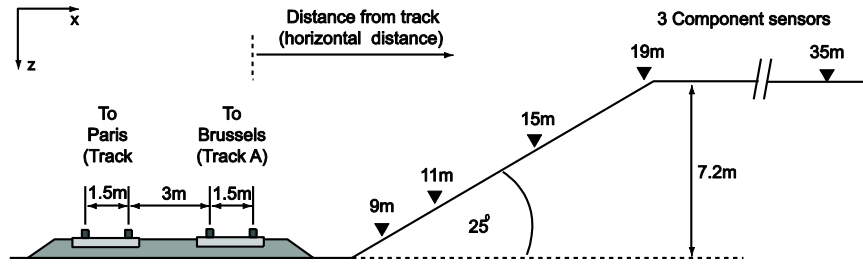


Fig. 8. Cutting track section geophone setup.



Fig. 9. Abutment site.

stiffer than the other two sites. A comparison between experimental the theoretical dispersion curves is shown in Fig. 18.

### 2.3.4. Soil damping calculation

Attenuation of vibration is primarily caused by material damping and geometrical damping. Geometrical damping describes the spreading of wave energy and is a function of soil geometry, while material damping describes the energy dissipation within soil particles. It has been shown that damping is dependent on excitation frequency [28], which can be described by hysteric damping using linear complex stiffness parameters.

Methods to assess damping profiles from experimental data include the half-power bandwidth method [4], phase and amplitude regression in the frequency-space domain [38], and frequency-wavenumber amplitude regression [45]. A challenge with these methods is that they depend on a very high coherence between signals. Therefore, [16,14] proposed an alternative solution which minimises the experimental and theoretical mobility (i.e. the velocity transfer functions). This approach is well suited to MASW testing and therefore was used (i.e. the damping calculations were performed by post-processing the data recorded during the hammer excitation rather than during train passage).

Fig. 19 compares the experimental and theoretical vertical mobilities for three different source-receiver positions using the damping profile shown Fig. 17a. Similar results were also obtained for sites 2 and 3. The agreement between experimental and theoretical results was found to be acceptable, despite small discrepancies between results. These discrepancies may have been caused by factors such as the anisotropic behavior of the soil, and have also been encountered by Refs. [2,16,41].

## 3. Results and discussion

### 3.1. General remarks

One of the aims of the experimental testing was to provide a series of vibration records that researchers could use for further

investigation and for the validation of numerical prediction models. One common assumption used for railway vibration modelling is that it is valid to model the problem using a linear system of equations. This reduces model complexity and is assumed valid because railway vibrations are often considered to generate low level strains. To investigate the validity of this assumption, the shear strain levels were investigated at each site. Shear strain levels were estimated from the experimental results using the equation [46]:

$$\gamma_i = \frac{PPV_i}{V_{s_i}}$$

where PPV was the peak particle velocity,  $\gamma$  was shear strain,  $V_s$  was the shear wave velocity of the upper soil layer and  $i$  was the measurement location.

Fig. 20 shows three best fit curves displaying how shear strain varied from the track. For each earthwork profile, the passage of five trains was considered and smoothed using higher order polynomials. It can be noticed that the shear strain is at a maximum at the nearest location to the track and reduces rapidly in the far field. This was expected as waves both loose energy due to material damping and spread energy due to radiation damping. Assuming the soil was a clay with plasticity index (PI=30%), it can be assumed to behave linearly for shear strains less than  $5 \times 10^{-3}\%$ . After this threshold, the soil will start to exhibit non-linear behaviour and at approximately  $5 \times 10^{-2}\%$  it will become highly non-linear [55]. As the maximum shear strain experienced at each site was much lower than this threshold ( $1.15 \times 10^{-3}\%$ ), it was evident that the soil at all measured locations was behaving in a visco-elastic manner.

### 3.2. Train speed

Fig. 21 shows the relationship between train speed and 'peak particle velocity' (PPV). Similarly, Fig. 22 shows the relationship between train speed and Velocity decibels (VdB). PPV was calculated as:

$$PPV = \max|v(t)|$$

where  $v(t)$  was the velocity time history. VdB was calculated as:

$$VdB = 20 \log_{10} \frac{v_{rms}}{v_0}$$

where  $v_{rms}$  was the root mean square of the time averaged signal (over a one second period), and  $v_0$  was the background level of vibration (assumed to be  $2.5 \times 10^{-8}$  m/s, [22]).

For each metric the response at both the near and far receivers was plotted along with a best fit line. It was found that there was a reasonably large scatter, particularly for the train passages on the near track. The standard deviation of PPV was  $6.4 \times 10^{-4}$  and  $4.4 \times 10^{-4}$  m/s, for the near and far tracks, respectively. Similarly, standard deviation of VdB was 2 and 1.5 dB, for the near and far tracks, respectively. It should be noted that a proportion of this may have been caused by differences in train load (passenger



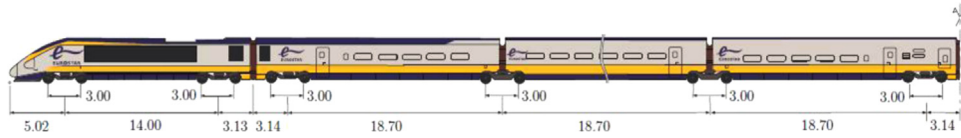


Fig. 13. Eurostar configuration.

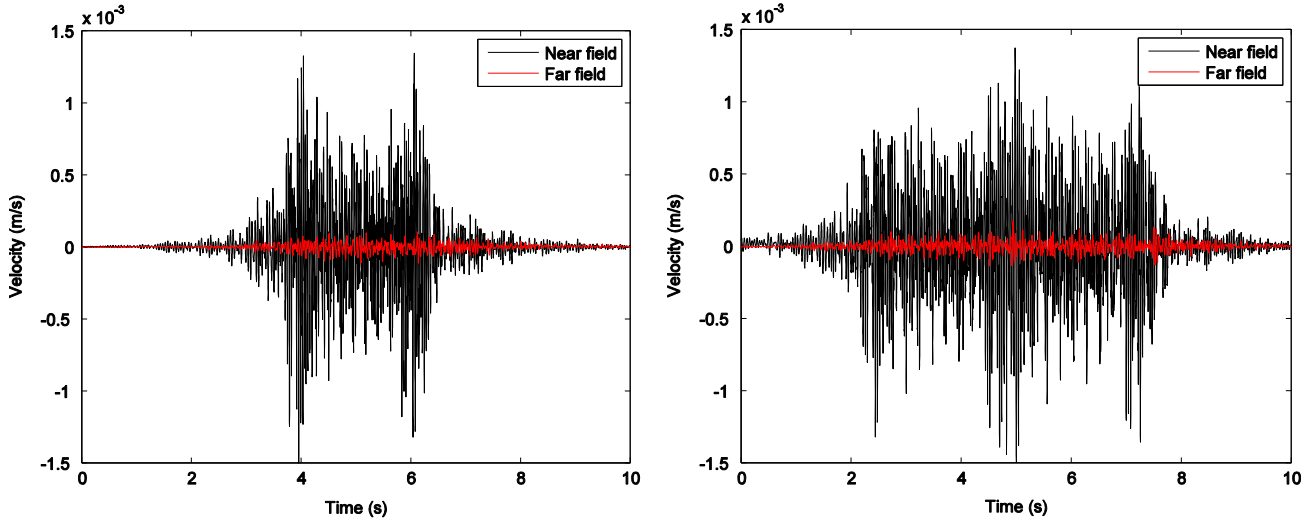


Fig. 14. Thalys vibration time histories left: Thalys single, right: Thalys double.

Table 3  
TGV properties.

	TGV	
	Driving	Passenger cars
Car body mass (kg)	55,790	24,000
Bogie mass (kg)	2,380	3,040
Wheelset mass (kg)	2,048	2,003
Primary suspension stiffness (MN/m)	2.45	1.4
Primary suspension damping (kNs/m)	20	120
Secondary suspension stiffness (MN/m)	2.45	0.45
Secondary suspension damping (kNs/m)	40	40

Table 4  
Thalys properties.

	Thalys		
	Bogie Y230A (driving car)	Bogie Y237A (lateral car)	Bogie Y237B (passenger car)
Car body mass (kg)	53,442	34,676	14,250
Bogie mass (kg)	3,261	8,156	1,400
Wheelset mass (kg)	2,009	2,009	2,050
Primary suspension stiffness (MN/m)	2.09	2.09	1.63
Primary suspension damping (kNs/m)	40	40	40
Secondary suspension stiffness (MN/m)	2.45	2.45	0.93
Secondary suspension damping (kNs/m)	40	40	40

3.6. Near vs far tracks

Fig. 28 compares average PPV vertical vibration levels for all trains passing on either the near or far tracks. The PPV levels from the far track were normalised by adding a 4.5 m offset to the receiver distances. This enabled a direct comparison between all 29 train passages.

In a similar manner to Fig. 27, it was found that the embankment case generated the lowest PPV levels while the cutting case

generated the highest. It is observed that the average vibration levels were similar for train passages on both the near and far tracks, however it was clear that for all three tracks, in the near field (< 15 m from the track) the far track vibration was lower than the near track vibration. The opposite was true as the distance from the track increased, with the far track showing elevated average PPV levels in comparison to the near track. This effect was particularly evident for the cutting earthworks profile. The cause of this rise in PPV was unknown.

**Table 5**  
Eurostar properties.

	Eurostar		
	Bogie Y230A (driving car)	Bogie Y237A (lateral car)	Bogie Y237B (passenger car)
Car body mass (kg)	54,166	33,854	27,083
Bogie mass (kg)	3,075	9,440	2,360
Wheelset mass (kg)	2,046	2,046	2,046
Primary suspension stiffness (MN/m)	2.63	2.20	2.07
Primary suspension damping (kNs/m)	12	12	12
Secondary suspension stiffness (MN/m)	3.26	0.91	0.61
Secondary suspension damping (kNs/m)	90	2	4

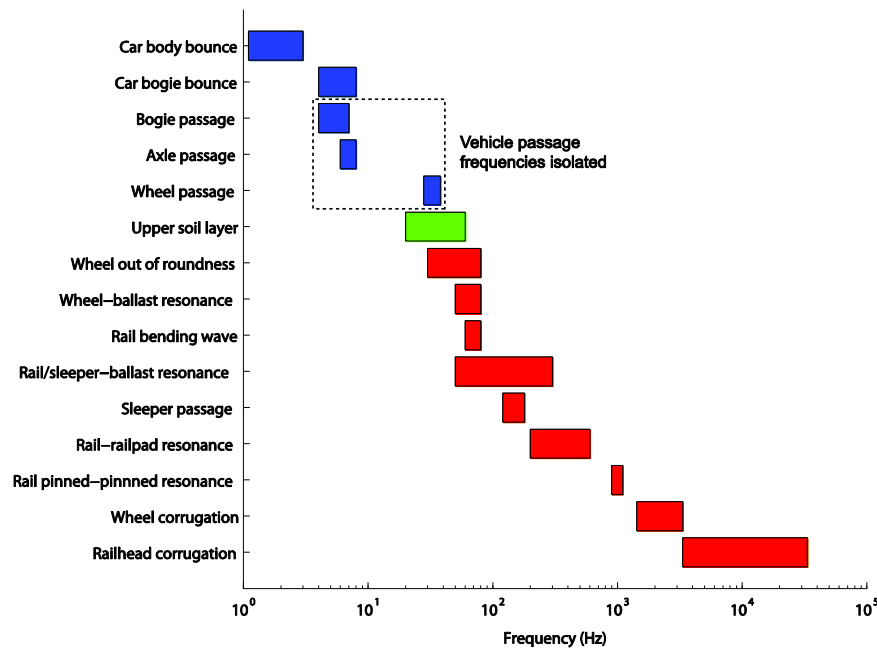


Fig. 15. Train, track and soil excitation mechanisms.

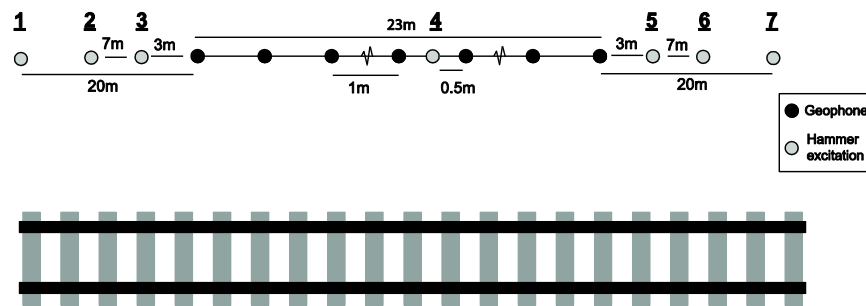


Fig. 16. MASW geophone configuration.

3.7. Far field vibration vs near field vibration

It is observed from Fig. 28 that vertical vibration levels decayed with distance from the excitation. This was as expected and was due to material and geometrical damping [5]. For the purpose of comparing near and far field vibration characteristics, Figs. 29–31 show how the normalised amplitude frequency content of vertical railway vibration varied from near to the far field (with 1/3 octave band histograms). For the at-grade case (Fig. 29) in the near field the frequency of propagating waves was predominantly between

15 and 30 Hz, with additional pronounced peaks at 27–31 Hz. In the far field the dominant frequency range was generally still located between 15 and 30 Hz although much less pronounced. A small resonant frequency at 8.8 Hz was visible in the near field and was greatly magnified in the far field.

For the embankment case (Fig. 30) in the near field the frequency range was much broader, and generally higher than the far field, with a key resonant frequency appearing at 141 Hz. The majority of near field frequency content was located below this peak, and similarly to the at-grade case there was a large

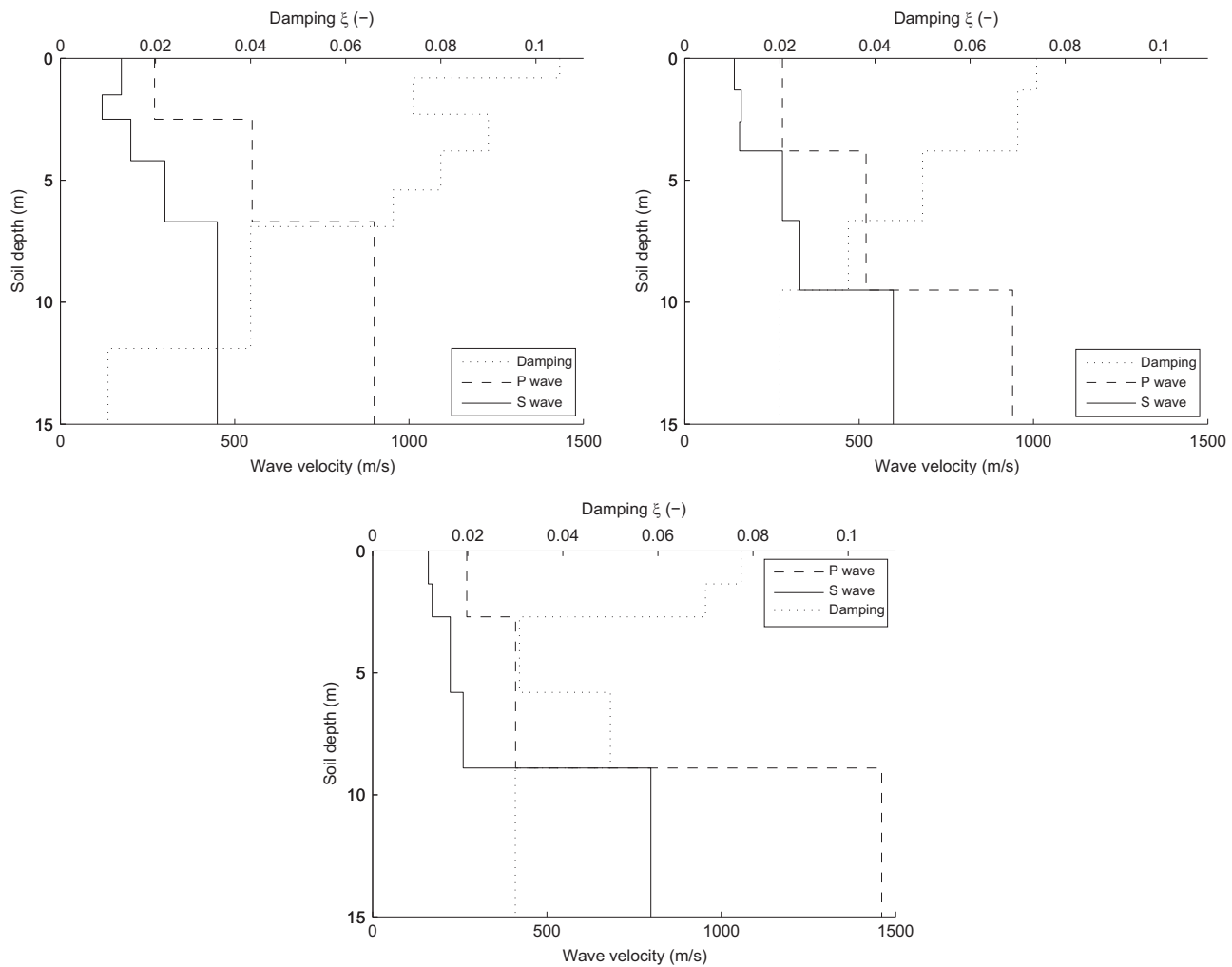


Fig. 17. Test site soil properties (left: at-grade, right: embankment, lower: cutting).

volume of waves propagating in the 15–30 Hz range. Additional zones of frequency content were also visible at 50–65 and 80–95 Hz. For the far field, a large percentage of this high frequency content had dissipated and the frequency content was located between 5 and 30 Hz. The main peak at 141 Hz had disappeared and three main peaks appeared at 8.6, 17.5 and 22 Hz.

These higher frequencies inside the embankment were in agreement with numerical results presented by Ref. [20]. It was postulated by [20] that these frequencies were generated due to the propagating waves reflecting off the edges of the embankment structure and a proportion of them becoming trapped within the embankment, in a similar manner to how guided waves behave. Similar conclusions were made regarding the experimental results in this study.

For the near field cutting case (Fig. 31) the frequency content also exhibited a greater spread in comparison to the at-grade case. The first major zone of frequency content was between 17 and 35 Hz, followed by another peak at 52 Hz and another smaller region of frequency content around 85 Hz. In comparison, a large percentage of the frequency content present in the near field was not visible in the far field results. The lower frequency content was bound in the region 8–35 Hz, with a significant eigenfrequency at 17 Hz. A low amplitude region of high frequency content was also visible around 130 Hz.

It was concluded from the frequency results that the near field vibration levels generated due the presence of an embankment

were of higher frequency in comparison to at-grade tracks. The frequency content of cuttings was also higher than the at-grade case but less so than the embankment case. It was also concluded that the high frequency vibrations generated by the track were damped rapidly as they propagated through the soil. This was because the frequency characteristics of soil typically prevent the propagation of high frequency vibration (Fig. 15). Instead, only the lower frequency waves, partly due to their longer wavelengths were able to propagate to larger distances.

### 3.8. Scattering due to abutments

Fig. 32 compares the variation in vibration levels with increasing distance from the track for both the abutment and non-abutment cases. At distances close to the track there was a large discrepancy between the vibration levels, however as the distance was increased to 35 m from the track, responses became similar. Although it cannot be proved, it is postulated that this 'shadow zone' occurred because the ground vibrations could not pass directly from the track into the ground due to the presence of the abutment. Instead the waves were forced to pass around the abutment before reaching the receivers. This travel path was longer thus causing the waves to lose a greater percentage of their energy due to damping.

Fig. 33 shows the difference in frequency content between the abutment and non-abutment cases. Although both responses were

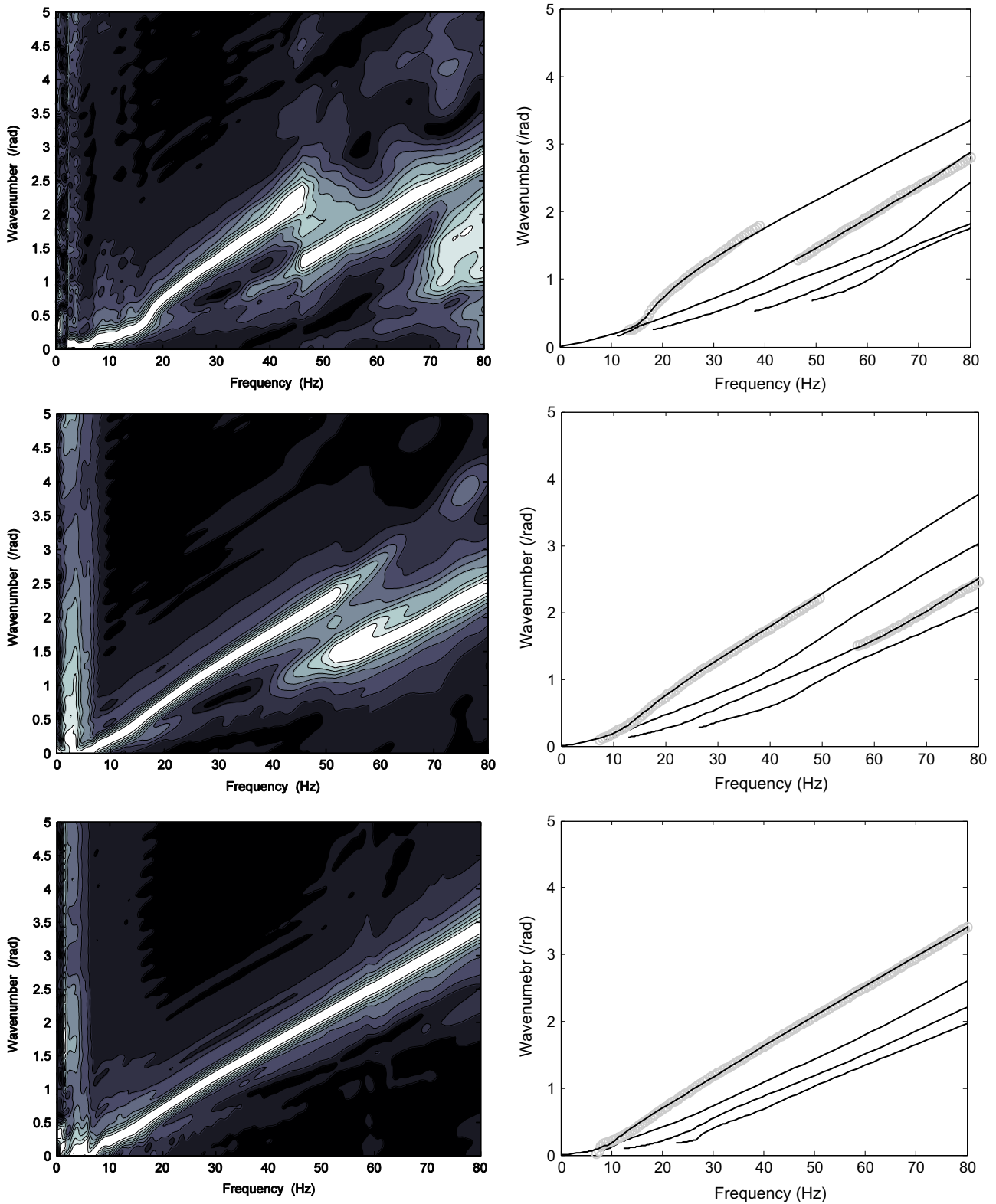


**Fig. 18.** Left: experimental dispersion curves, right: theoretical dispersion curves (black solid lines) vs experimental (grey circles), top: at-grade site, middle: embankment site, bottom: cutting site.

similar, the frequency spectrum for the abutment case was wider and a greater number of peaks were present. This occurred due to the complex wave scattering process induced by the abutment dimensions. When the waves generated by train passed through the track they were scattered due to the complex geometry of the abutment, thus generating a wider frequency spectrum.

### 3.9. Discussion

The results presented in this work are useful for environmental consultants and modellers, railway constructors, railway operators, real estate owners, asset managers and academic researchers (e.g. Universities and research institutes). They will allow for the

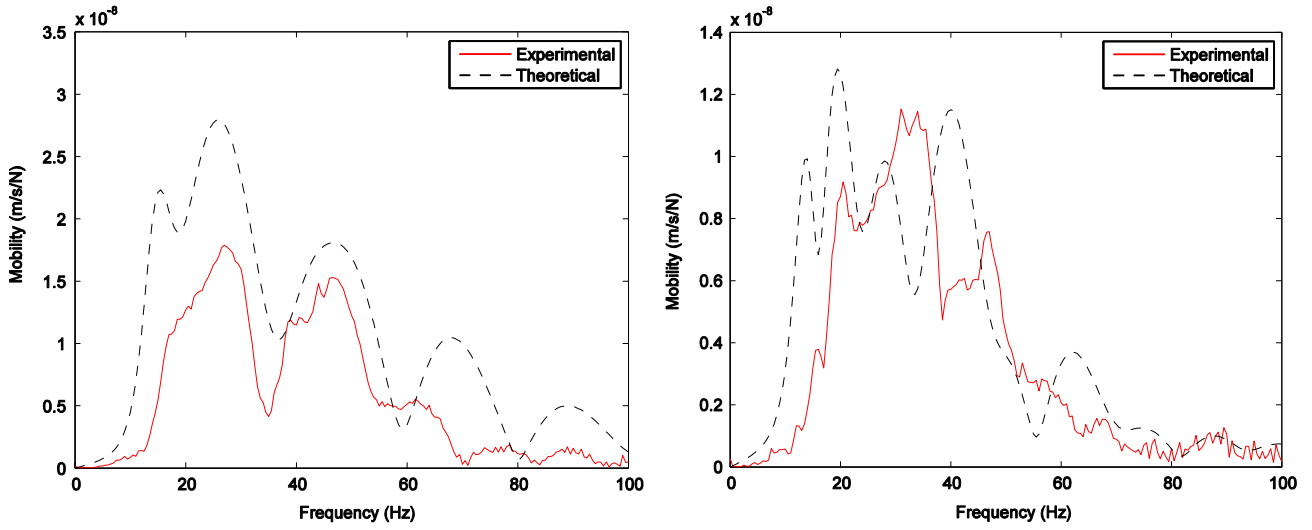


Fig. 19. Vertical mobility of site 1 for two different distances between source-receiver, left: 15 m, right: 20 m.

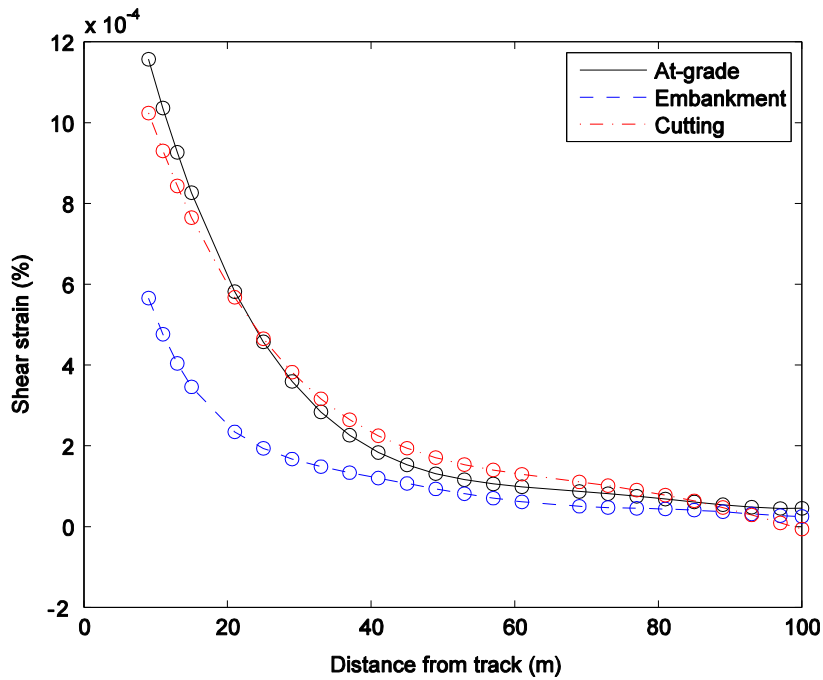


Fig. 20. Vertical shear strain variation with distance from track.

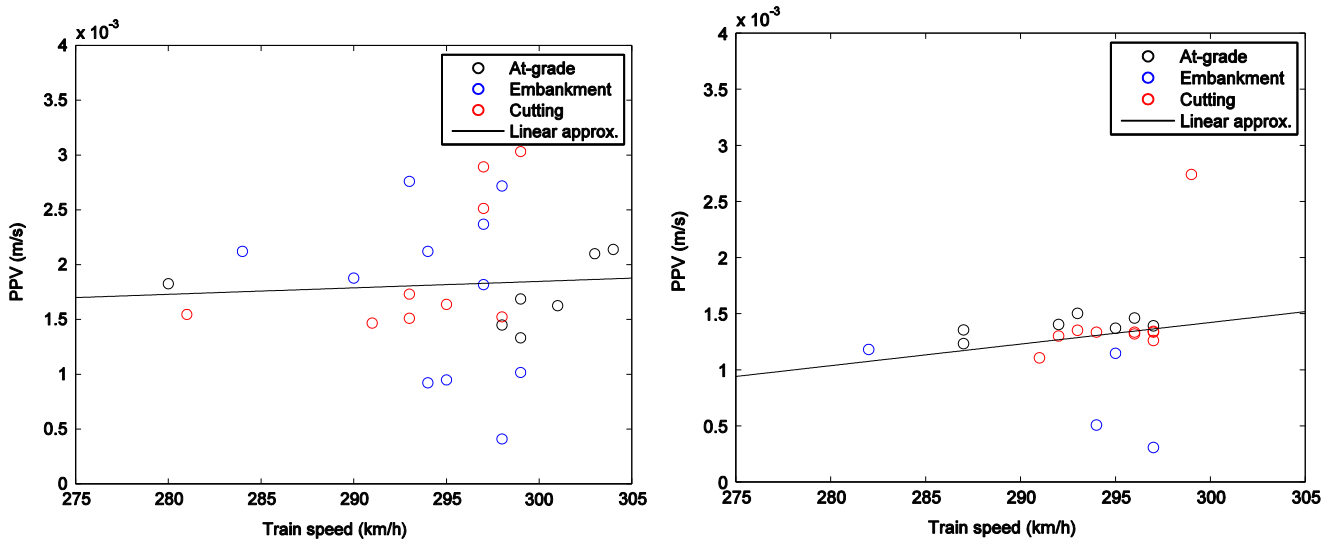


Fig. 21. The effect of train speed on PPV, left: near track, right: far track.

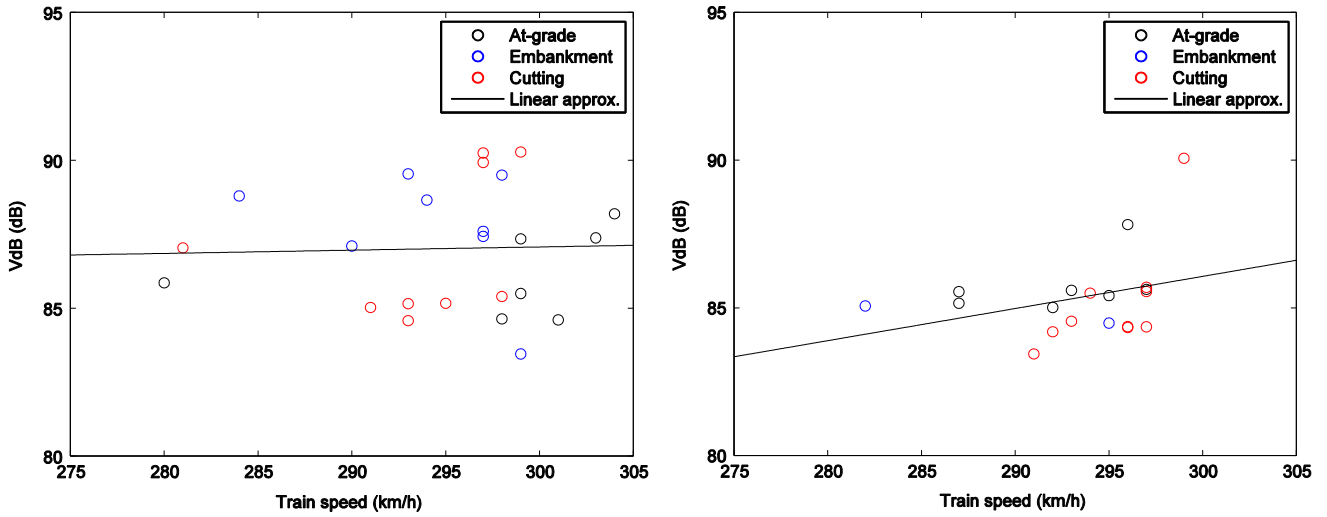


Fig. 22. The effect of train speed on VdB, left: near track, right: far track.

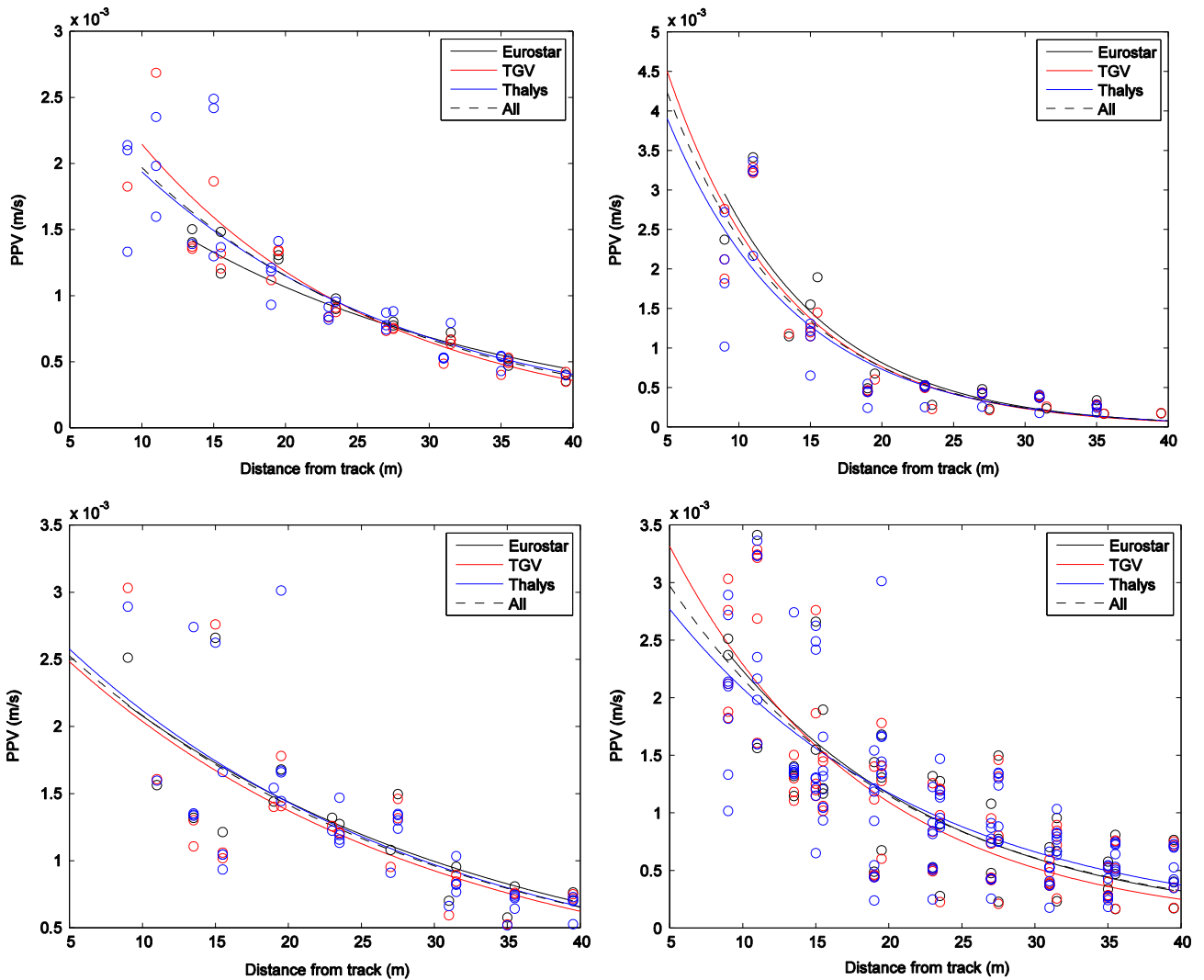


Fig. 23. Vertical vibration levels for various train types, top left: at-grade, top right: embankment, bottom left: cutting, bottom right: all sites.

validation of new and existing vibration prediction models and provide interesting insights into vibration propagation characteristics within different earthwork profiles.

In particular, a key finding was that the repeatability of experiments was lower than anticipated and trains travelling at the same speed, on the same track generated variances in

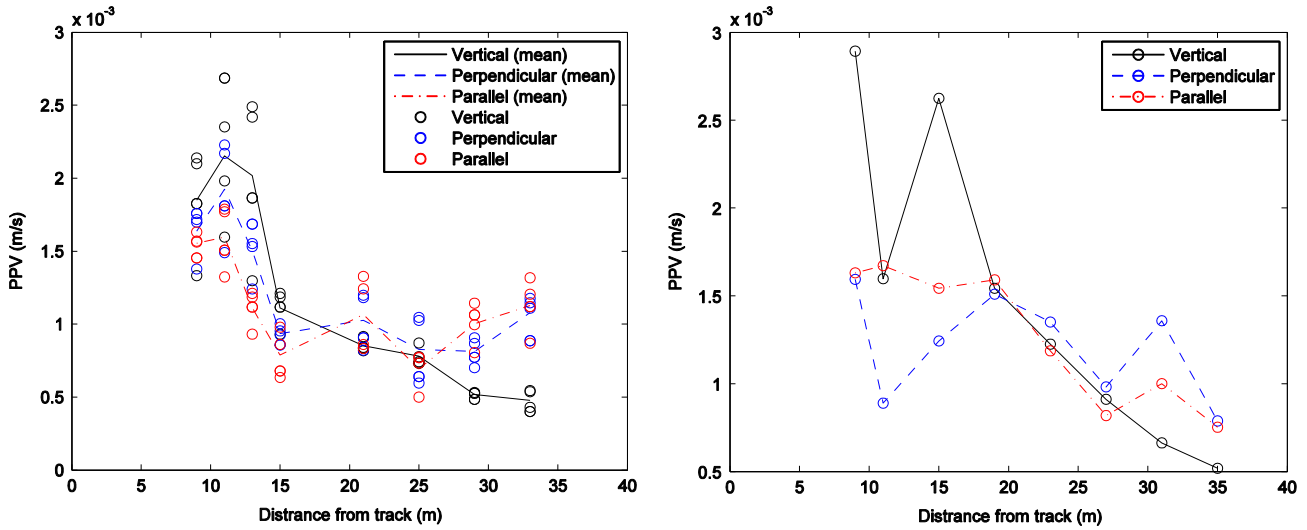


Fig. 24. Three component PPV levels for at-grade track, left: mean PPV for all trains on near track, right: individual Thalys passage at 299 km/h on near track.

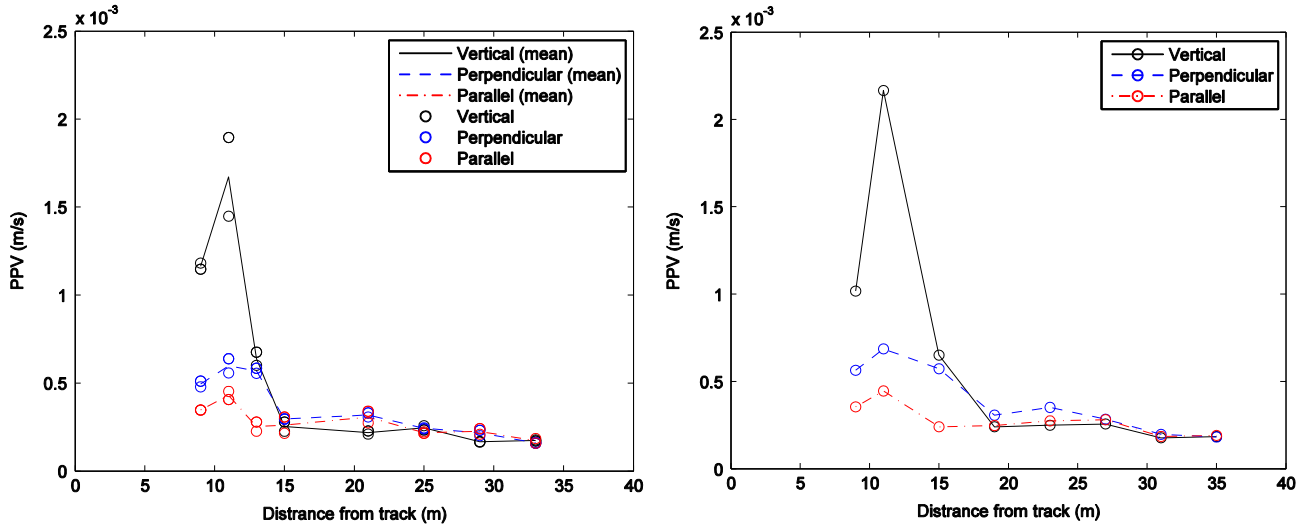


Fig. 25. Three component PPV levels for embankment track, left: mean levels for all trains on far track, right: Individual Thalys passage at 299 km/h on near track.

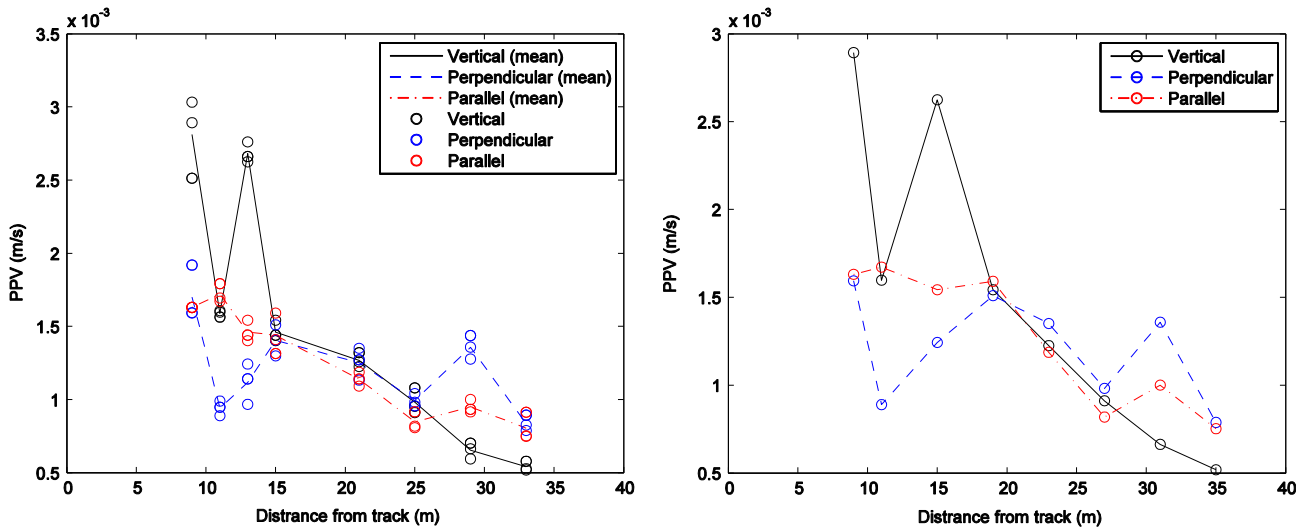


Fig. 26. Three component PPV levels for cutting track, left: mean levels for all trains on near track, right: individual Thalys passage at 297 km/h on near track.

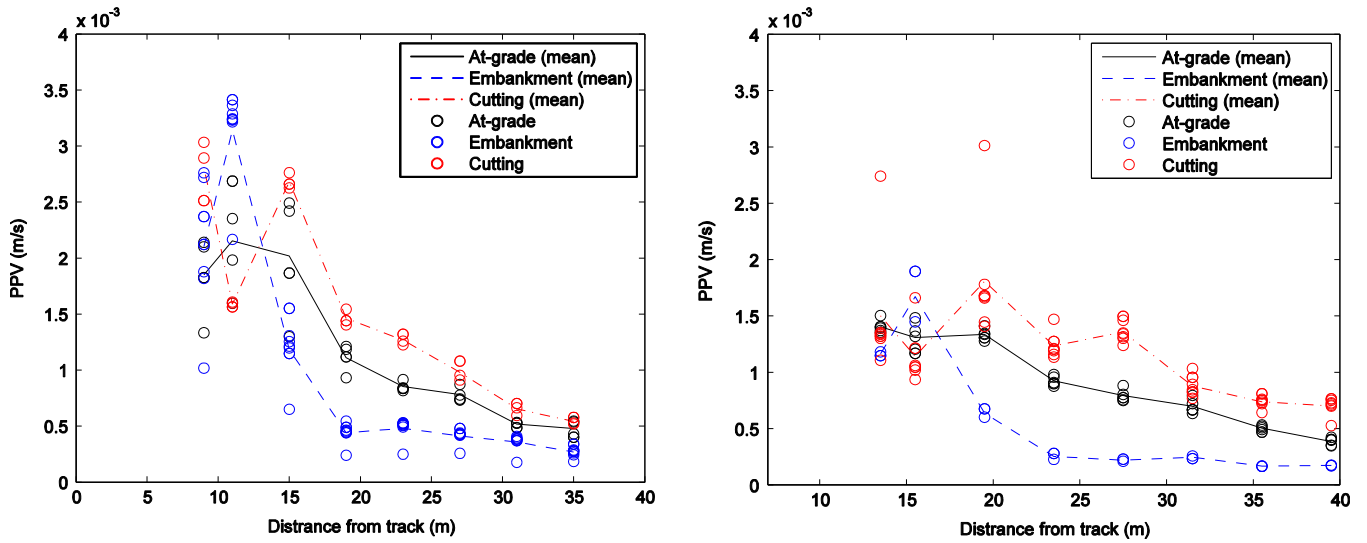


Fig. 27. Earthworks profile effects in the vertical direction, top: near track, bottom: far track.

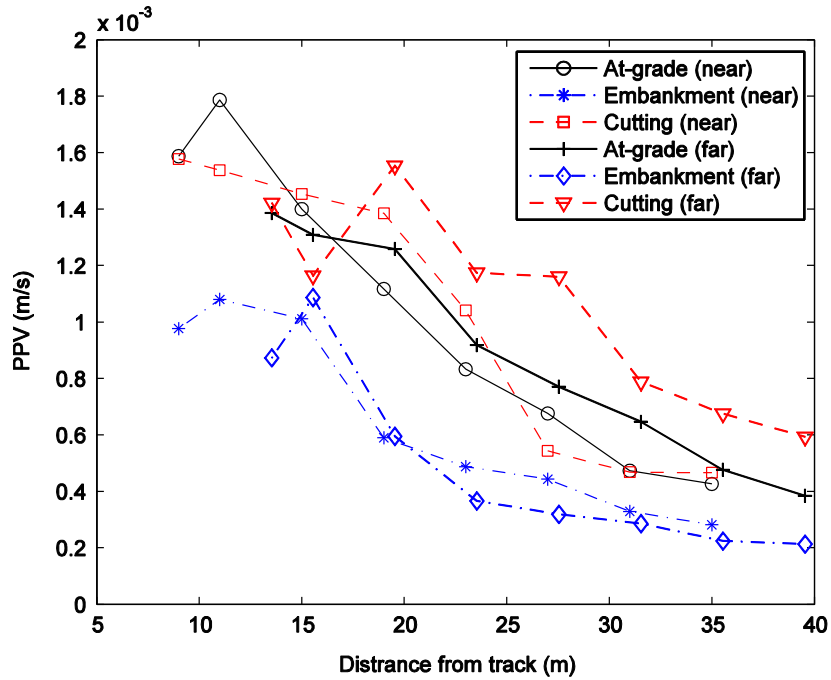


Fig. 28. Vertical vibration levels generated due to near and far train passages.

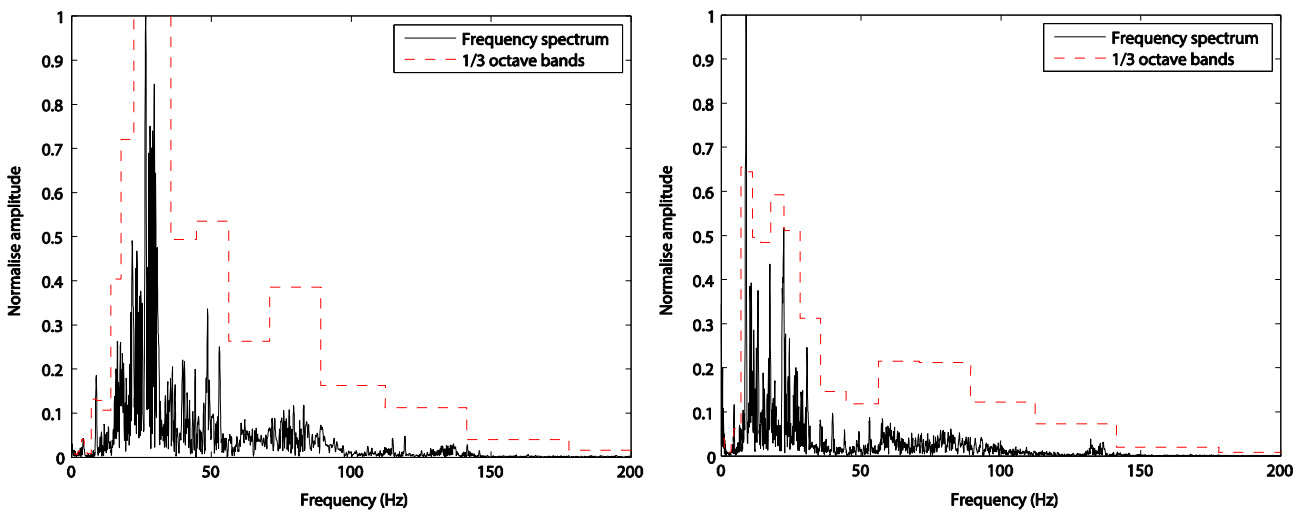


Fig. 29. Frequency spectrum at at-grade site (left: near, right: far).

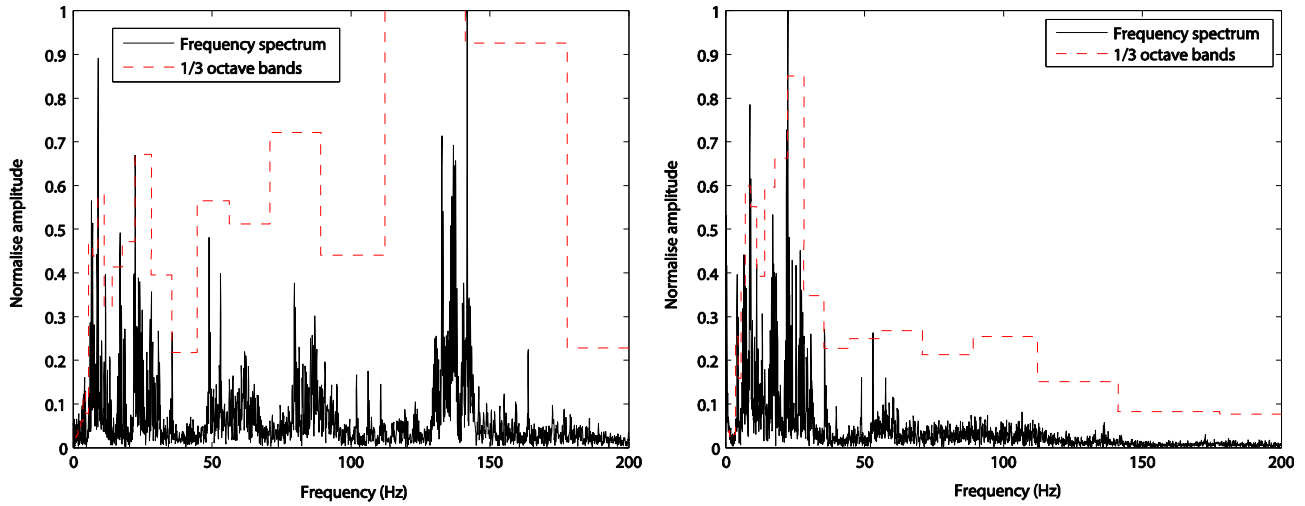


Fig. 30. Frequency spectrum at embankment (left: near, right: far).

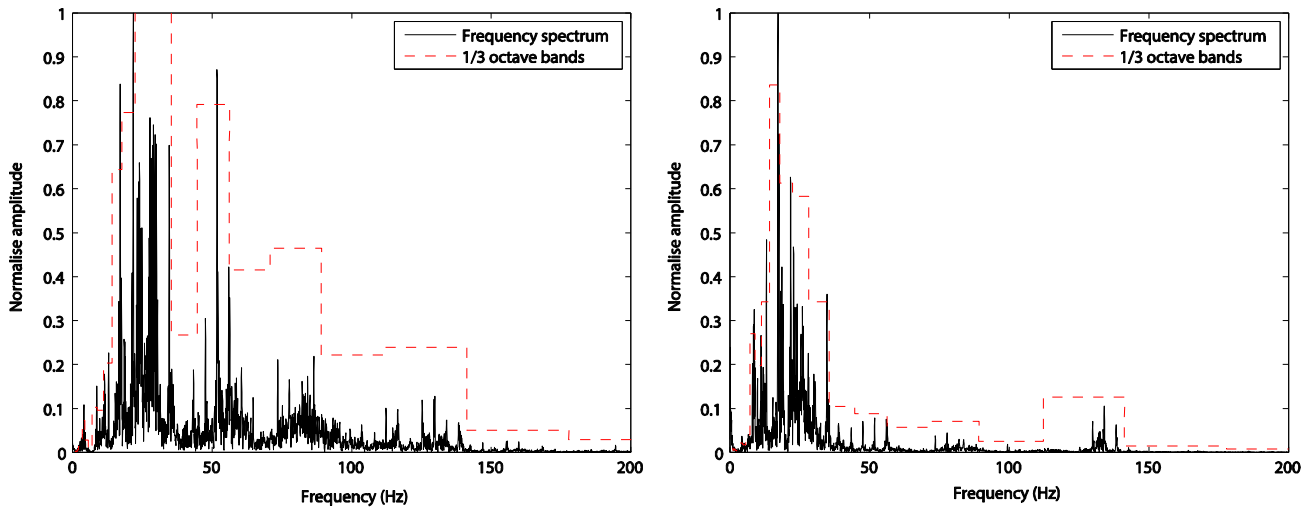


Fig. 31. Frequency spectrum at cutting (left: near, right: far).

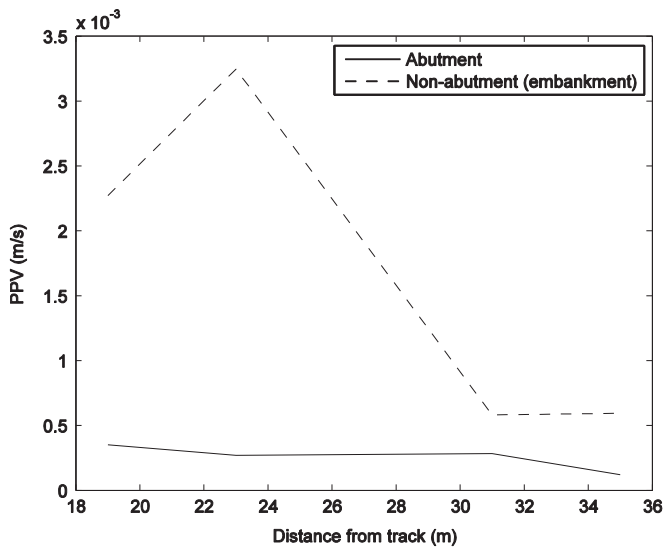


Fig. 32. Vertical vibration variation (abutment).

effective, it is important that there are trends and a degree of repeatability between results. As expected, trends were found in the experimental analysis performed in this work, thus justifying the application of numerical modelling for railway vibration problems. Despite this, although justified, due to ground vibration uncertainty, in practice prediction is undertaken using a conservative approach, thus highlighting future research needs in this area to better quantify the expected levels of risk for individual projects.

Another notable finding was that vertical vibrations were not always the most dominant form of vibration. Instead, horizontal vibrations were found to be just as important. Once again, this is relevant for numerical modelling which typically relies on solely predicting vertical vibrations.

Lastly, PPV levels were found to be similar for all train types. This was likely because the characteristics of three train types measured (Eurostar, TGV and Thalys) were similar (e.g. wheel spacings, weights, configuration...etc.). Despite this, for alternative metrics (rather than PPV) that account for the time duration of a signal (e.g.  $KB_{fmax}$ —[19]) this may not have been the case. This is likely to be because trains such as the Eurostar commonly have twice number of carriages as Thalys, thus generating a longer duration of vibration and possibly causing an increase in these alternative metrics.

vibration levels. This is pertinent for numerical modelling, which irrespective of discipline, commonly has to deal with innately large scatter and uncertainty. For numerical modelling to be

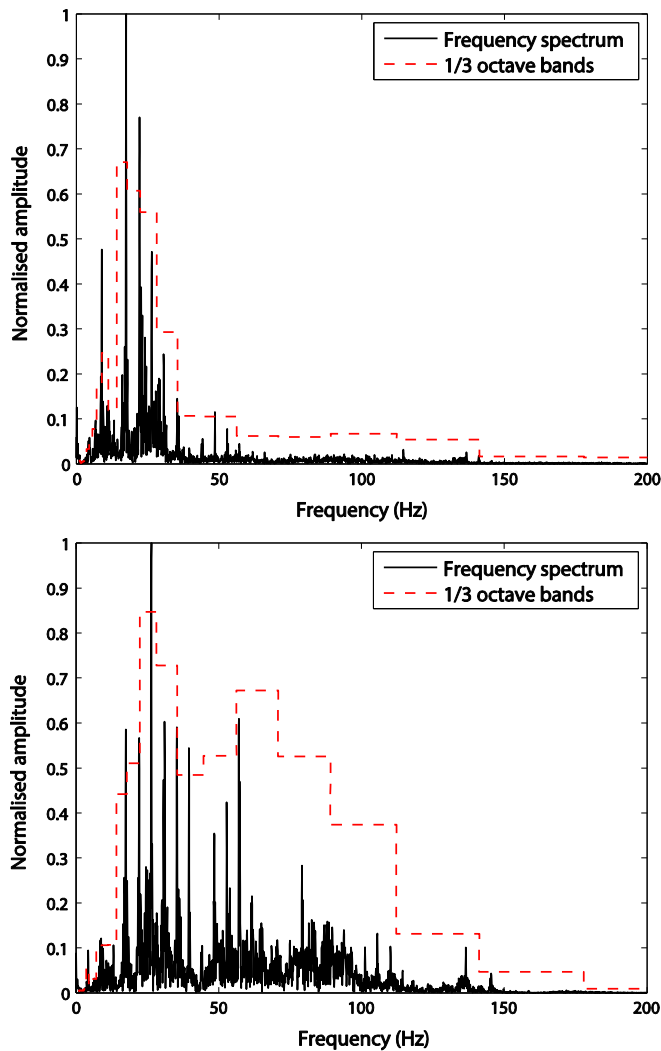


Fig. 33. Frequency spectrum comparison (top: no abutment, bottom: abutment).

#### 4. Conclusions

Field experiments were undertaken at 4 railway sites across Belgium for the purpose of providing researchers with a freely available dataset for modelling validation, and to provide new insights into railway ground vibrations. The experiments consisted of ground vibration monitoring to assess vibration levels due to train passage, and MASW tests to determine the underlying soil properties. MASW tests were used to determine S-wave and P-wave velocities and the results were validated using refraction analysis. Train passage data can be found in the download section of: [www.davidpconnolly.com/](http://www.davidpconnolly.com/).

Analysis of the field results revealed that:

- i. Vertical component vibration levels from high speed trains were of higher amplitude than horizontal vibration levels at locations close to the track. However, as distance increased, the horizontal vibration levels were similar in magnitude and in some cases were more dominant.
- ii. There was a large scatter between train speed and vibration level data. A low, but positive correlation between variables was tentatively proposed.
- iii. The cutting site generated elevated levels of ground vibration in comparison to at-grade and fill embankment track sections.

- iv. The embankment site caused the generation of higher frequency content in comparison to at-grade track. The cutting also generated higher frequency content than at-grade sections, albeit less than embankments.
- v. The higher frequency components generated on all tracks was damped rapidly as the waves propagate through the soil. Lower frequency components attenuated less quickly.
- vi. Thalys, TGV and Eurostar trains generate similar levels of ground vibration.

#### Acknowledgements

The authors wish to thank the railway operator Infrabel, and especially M. Debruxelles and M. Demaret, for their support during the experimental investigations, and all data provided related to the train/track characteristics. Acknowledgement also goes to the University of Edinburgh, the Université de Mons, Heriot Watt University and the University of Porto for the support and resources provided for the undertaking of this research. Additionally, the funding provided by Engineering and Physical Sciences Research Council UK (EP/H029397/1), Natural Environment Research Council (UK) and “FCT—Fundação para a Ciência e Tecnologia”, Portugal, (research project—PTDC/ECM/114505/2009), is also greatly appreciated, without which, this research could not have been undertaken. Lastly, thanks is given to M. Percival and M. Scoubeau who provided vital experimental assistance. The data associated with this research can be found via [9].

#### Appendix

See Tables 6 and 7.

Table 6  
Soil wave speeds.

Site 1			Site 2			Site 3		
<i>h</i> (m)	<i>V<sub>s</sub></i> (m/s)	<i>V<sub>p</sub></i> (m/s)	<i>h</i> (m)	<i>V<sub>s</sub></i> (m/s)	<i>V<sub>p</sub></i> (m/s)	<i>h</i> (m)	<i>V<sub>s</sub></i> (m/s)	<i>V<sub>p</sub></i> (m/s)
1.5	175	270	1.3	142	280	1.35	160	270
1	120	270	1.3	162	280	1.35	171	270
1.7	202	550	1.2	157	280	3.1	223	410
2.5	300	550	2.85	280	520	3.1	260	410
Inf.	450	900	2.85	330	520	Inf.	798	1460
			Inf.	598	940			

Table 7  
Soil damping.

Site 1		Site 2		Site 3	
Layer thickness (m)	Damping (–)	Layer thickness (m)	Damping (–)	Layer thickness (m)	Damping (–)
0.8	0.105	1.3	0.074	1.35	0.0775
1.5	0.0742	2.5	0.07	1.35	0.07
1.5	0.09	2.85	0.05	3.1	0.0309
1.6	0.08	2.85	0.0344	3.1	0.05
1.5	0.07	Inf.	0.02	Inf.	0.03
5	0.04				
	0.01				

## References

- [1] Andersen L, Jones CJC. Coupled boundary and finite element analysis of vibration from railway tunnels—a comparison of two- and three-dimensional models. *J Sound Vib* 2006;293(3–5):611–25. <http://dx.doi.org/10.1016/j.jsv.2005.08.044>.
- [2] Auersch L. Wave propagation in layered soils: theoretical solution in wave-number domain and experimental results of hammer and railway traffic excitation. *J Sound Vib* 1994;173(2):233–64.
- [3] Auersch L. Train induced ground vibrations: different amplitude-speed relations for two layered soils. *Proc Inst Mech Eng Part F J Rail Rapid Transit* 2012;226(5):469–88. <http://dx.doi.org/10.1177/0954409712437305>.
- [4] Badsar Sa, Schevenels M, Haegeman W, Degrande G. Determination of the material damping ratio in the soil from SASW tests using the half-power bandwidth method. *Geophys J Int* 2010;182(3):1493–508. <http://dx.doi.org/10.1111/j.1365-246X.2010.04690.x>.
- [5] Barkan M. Dynamics of bases and foundations. New York, US: McGraw-Hill Inc.; 1962; 1–496.
- [6] Campos J, de Rus G. Some stylized facts about high-speed rail: a review of HSR experiences around the world. *Transp Policy* 2009;16(1):19–28. <http://dx.doi.org/10.1016/j.tranpol.2009.02.008>.
- [7] Connolly D, Giannopoulos A, Fan W, Woodward PK, Forde MC. Optimising low acoustic impedance back-fill material wave barrier dimensions to shield structures from ground borne high speed rail vibrations. *Constr Build Mater* 2013;44:557–64. <http://dx.doi.org/10.1016/j.conbuildmat.2013.03.034>.
- [8] Connolly D, Giannopoulos A, Forde MC. Numerical modelling of ground borne vibrations from high speed rail lines on embankments. *Soil Dyn Earthquake Eng* 2013;46:13–9. <http://dx.doi.org/10.1016/j.soildyn.2012.12.003>.
- [9] Connolly, DP. High speed rail testing—experimental vibration data (davidpconnolly.com). (<http://www.davidpconnolly.com/>); 2014.
- [10] Connolly, DP, Kouroussis, G, Fan, W, Percival, M, Giannopoulos, A, Woodward, PK, et al. An experimental analysis of embankment vibrations due to high speed rail. In: Proceedings of the 12th international railway engineering conference; 2013.
- [11] Connolly DP, Kouroussis G, Giannopoulos A, Verlinden O, Woodward PK, Forde MC. Assessment of railway vibrations using an efficient scoping model. *Soil Dyn Earthquake Eng* 2014;58:37–47. <http://dx.doi.org/10.1016/j.soildyn.2013.12.003>.
- [12] Connolly DP, Kouroussis G, Laghrouche O, Ho CL, Forde MC. Benchmarking railway vibrations—track, vehicle, ground and building effects. *Constr Build Mater* 2014. <http://dx.doi.org/10.1016/j.conbuildmat.2014.07.042>.
- [13] Connolly DP, Kouroussis G, Woodward PK, Giannopoulos A, Verlinden O, Forde MC. Scoping prediction of re-radiated ground-borne noise and vibration near high speed rail lines with variable soils. *Soil Dyn Earthquake Eng* 2014;66(2014):78–88. <http://dx.doi.org/10.1016/j.soildyn.2014.06.021>.
- [14] Costa PA, Calcada R, Cardoso A. Vibrations induced by railway traffic: prediction, measurement and mitigation. Traffic induced environmental vibrations and controls: theory and application 2013:49–89.
- [15] Costa PA, Calcada R, Cardoso AS. Influence of train dynamic modelling strategy on the prediction of track-ground vibrations induced by railway traffic. *Proc Inst Mech Eng Part F J Rail Rapid Transit* 2012;226(4):434–50. <http://dx.doi.org/10.1177/0954409711433686>.
- [16] Costa PA, Calcada R, Cardoso AS. Track-ground vibrations induced by railway traffic: in-situ measurements and validation of a 2.5D FEM-BEM model. *Soil Dyn Earthquake Eng* 2012;32(1):111–28.
- [17] Costa PA, Calcada R, Cardoso AS, Bodare A. Influence of soil non-linearity on the dynamic response of high-speed railway tracks. *Soil Dyn Earthquake Eng* 2010;30:221–35. <http://dx.doi.org/10.1016/j.soildyn.2009.11.002>.
- [18] Degrande G, Schillekens L. Free field vibrations during the passage of a Thalys high-speed train at variable speed. *J Sound Vib* 2001;247(1):131–44. <http://dx.doi.org/10.1006/jsvi.2001.3718>.
- [19] Deutsches Institut für Normung. DIN 4150-2—human exposure to vibration in buildings. International Standards Organisation 1999:1–63.
- [20] Ditzel A, Herman G. The influence of a rail embankment on the vibrations generated by moving trains. *J Sound Vib* 2004;271:937–57. [http://dx.doi.org/10.1016/S0022-460X\(03\)00772-7](http://dx.doi.org/10.1016/S0022-460X(03)00772-7).
- [21] El Kacimi A, Woodward PK, Laghrouche O, Medero G. Time domain 3D finite element modelling of train-induced vibration at high speed. *Comput Struct* 2013;118:66–73. <http://dx.doi.org/10.1016/j.compstruc.2012.07.011>.
- [22] Federal Railroad Administration. High-speed ground transportation noise and vibration impact assessment. U.S. Department of Transportation 2012:1–248.
- [23] Ferrara, R, Leonardi, G, Jourdan, F. A two-dimensional numerical model to analyze the critical velocity of high speed infrastructure the 2D numerical model. In: Proceedings of the 14th international conference on civil, structural and environmental engineering computing; 2013. p. 1–16.
- [24] Fryba L. Vibration of solids and structures under moving loads. Groningen: The Netherlands: Noordhoff International Publishing; 1972; 1–524.
- [25] Galvin P, Domínguez J. Experimental and numerical analyses of vibrations induced by high-speed trains on the Córdoba–Málaga line. *Soil Dyn Earthquake Eng* 2009;29(4):641–57. <http://dx.doi.org/10.1016/j.soildyn.2008.07.001>.
- [26] Galvin P, Romero A, Domínguez J. Fully three-dimensional analysis of high-speed train-track-soil-structure dynamic interaction. *J Sound Vib* 2010;329(24):5147–63. <http://dx.doi.org/10.1016/j.jsv.2010.06.016>.
- [27] Gupta S, Van den Bergh H, Lombaert G, Degrande G. Numerical modelling of vibrations from a Thalys high speed train in the Groene Hart tunnel. *Soil Dyn Earthquake Eng* 2010;30(3):82–97. <http://dx.doi.org/10.1016/j.soildyn.2009.09.004>.
- [28] Hardin B. The nature of damping in sands. *J Soil Mech Found Div* 1965;91:63–97.
- [29] Hussein MFM, Hunt HEM. A numerical model for calculating vibration due to a harmonic moving load on a floating-slab track with discontinuous slabs in an underground railway tunnel. *J Sound Vib* 2009;321(1–2):363–74. <http://dx.doi.org/10.1016/j.jsv.2008.09.023>.
- [30] Hussein M, Hunt HEM, Kuo K, Costa PA, Barbosa J. The use of sub-modelling technique to calculate vibration in buildings from underground railways. *Proc Inst Mech Eng Part F J Rail Rapid Transit* 2013. <http://dx.doi.org/10.1177/0954409713511449>.
- [31] Kogut, J, Degrande, G, Haegeman, W, Karl, L. Free field vibration due to the passage of an IC train and a Thalys HST on the high speed track L2 Brussels-Koln. IABSE symposium report; 2002. <http://dx.doi.org/10.2749/222137803796330176>.
- [32] Kouroussis G. Mesures de vibrations induites sur l'environnement par le passage de trains à grande vitesse. Faculte Polytechnique De Mons 2005:1–84 (Technical report).
- [33] Kouroussis, G, Connolly, DP, Forde, MC, Verlinden, O. An experimental study of embankment conditions on high-speed railway ground vibrations. In: International congress on sound and vibration (ICSV20). Bangkok, Thailand; 2013. p. 1–8.
- [34] Kouroussis G, Connolly DP, Forde MC, Verlinden O. Train speed calculation using ground vibrations. *Proc Inst Mech Eng Part F J Rail Rapid Transit* 2014;0(0):1–18. <http://dx.doi.org/10.1177/0954409713515649>.
- [35] Kouroussis G, Connolly DP, Verlinden O. Railway induced ground vibrations—a review of vehicle effects. *Int J Rail Transp* 2014;2(2):69–110. <http://dx.doi.org/10.1080/23248378.2014.897791>.
- [36] Kouroussis G, Verlinden O, Conti C. Free field vibrations caused by high-speed lines: measurement and time domain simulation. *Soil Dyn Earthquake Eng* 2011;31(4):692–707. <http://dx.doi.org/10.1016/j.soildyn.2010.11.012>.
- [37] Krylov V. Generation of ground vibrations by superfast trains. *Appl Acoust* 1995;44(2):149–64. [http://dx.doi.org/10.1016/0003-682X\(95\)91370-1](http://dx.doi.org/10.1016/0003-682X(95)91370-1).
- [38] Lai C. Simultaneous measurement and inversion of surface wave dispersion and attenuation curves. *Soil Dyn Earthquake Eng* 2002;22(9–12):923–30. [http://dx.doi.org/10.1016/S0267-7261\(02\)00116-1](http://dx.doi.org/10.1016/S0267-7261(02)00116-1).
- [39] Ling X-Z, Chen S-J, Zhu Z-Y, Zhang F, Wang L-N, Zou Z-Y. Field monitoring on the train-induced vibration response of track structure in the Beiluhe permafrost region along Qinghai–Tibet railway in China. *Cold Reg Sci Technol* 2010;60(1):75–83. <http://dx.doi.org/10.1016/j.coldregions.2009.08.005>.
- [40] Lombaert G, Degrande G. Ground-borne vibration due to static and dynamic axle loads of InterCity and high-speed trains. *J Sound Vib* 2009;319:1036–66. <http://dx.doi.org/10.1016/j.jsv.2008.07.003>.
- [41] Lombaert G, Degrande G, Kogut J, Francois S. The experimental validation of a numerical model for the prediction of railway induced vibrations. *J Sound Vib* 2006;297(3–5):512–35. <http://dx.doi.org/10.1016/j.jsv.2006.03.048>.
- [42] Lopes P, Costa PA, Ferraz M, Calcada R, Cardoso AS. Numerical modelling of vibrations induced by railway traffic in tunnels: from the source to the nearby buildings. *Soil Dyn Earthquake Eng* 2014;61–62:269–85. <http://dx.doi.org/10.1016/j.soildyn.2014.02.013>.
- [43] Madhus C. High-speed railway lines on soft ground: dynamic behaviour at critical train speed. *J Sound Vib* 2000;231(3):689–701. <http://dx.doi.org/10.1006/jsvi.1999.2647>.
- [44] Park Seismic. Multichannel analysis of surface waves. Retrieved from www.masw.com; 2013.
- [45] Petyt M, Thompson DJ, Jones CJC. A model for ground vibration from railway tunnels. *Proc Inst Civ Eng Transp* 2002;153(2):121–9. <http://dx.doi.org/10.1680/tran.2002.153.2.121>.
- [46] Rix G, Lai C, Wesley-Spang A. In situ measurement of damping ratio using surface waves. *J Geotech Geoenviron Eng* 2000;126(5):472–80.
- [47] Sheng X, Jones CJC, Petyt M. Ground vibration generated by a harmonic load acting on a railway track. *J Sound Vib* 1999;225(1):3–28. <http://dx.doi.org/10.1006/jsvi.1999.2232>.
- [48] Stiebel D. Protocol for free field measurement of mitigation effects (RIVAS—Deliverable D1.2) 2011:1–25.
- [49] Stiebel D, Muller R, Bongini E, Ekbal A, Coquel G, Alguacil AA. Definition of reference cases typical for hot-spots in Europe with existing vibration problems (RIVAS—Deliverable D1.5) 2012:1–16.
- [50] Thompson D. Railway noise and vibration. Mechanisms, modelling and means of control. Oxford, UK: Elsevier Ltd.; 2009; 1–532.
- [51] Varandas JN, Hölscher P, Silva MaG. Dynamic behaviour of railway tracks on transitions zones. *Comput Struct* 2011;89(13–14):1468–79. <http://dx.doi.org/10.1016/j.compstruc.2011.02.013>.
- [52] Wang J, Jin X, Cao Y. High speed Maglev train-guideway-tunnel-soil modelling of ground vibration. *J Rail Rapid Transit* 2011. <http://dx.doi.org/10.1177/0954409711424823>.
- [53] Wathelet M. An improved neighborhood algorithm: parameter conditions and dynamic scaling. *Geophys Res Lett* 2008;35(9):1–5. <http://dx.doi.org/10.1029/2008GL033256>.
- [54] Wathelet, M. www.Geopsy.org; 2008b.
- [55] Wood DM. Soil behaviour and critical state soil mechanics. Cambridge, UK: Cambridge University Press; 1990; 462.